Particuology 42 (2019) 92–103

Contents lists available at ScienceDirect

Particuology

journal homepage: www.elsevier.com/locate/partic

Simulation of spray coating in a spouted bed using recurrence CFD

Paul Kieckhefen[a,*], Thomas Lichtenegger[b,c], Swantje Pietsch[a], Stefan Pirker[b], Stefan Heinrich[a]

[a] Institute of Solids Process Engineering and Particle Technology, Hamburg University of Technology, Hamburg, Germany
[b] Department for Particulate Flow Modelling, Johannes Kepler University, Linz, Austria
[c] Linz Institute of Technology (LIT), Johannes Kepler University, Linz, Austria

ARTICLE INFO

Article history:
Received 1 November 2017
Received in revised form 5 January 2018
Accepted 16 January 2018
Available online 25 June 2018

Keywords:
CFD–DEM
Recurrence CFD
Spray coating
Time-scale decoupling
Spouted bed
Draft plate

ABSTRACT

Although numerical models such as the computational fluid dynamics–discrete element method (CFD–DEM) have enabled the accurate simulation of laboratory-scale apparatuses, the application of these methods to large-scale apparatuses with many particles and time scales ranging from minutes to hours remains a challenge. The recently developed recurrence CFD (rCFD) method seeks to overcome these issues in pseudo-periodic processes by extrapolating globally recurring patterns in a physically meaningful way and describing the transport and interaction of passive scalars using Lagrangian tracers. Spouted beds represent an interesting target because of the associated variety of flow regimes. They can be effectively described by CFD–DEM on the time scale of tens of seconds, whereas industrially relevant processes typically take hours. In this contribution, we established the validity of applying the Lagrangian rCFD method to spouted beds by demonstrating the accurate reproduction of the particle residence time distribution in a fictitious spray zone. The deposition of spray droplets onto tracer particles was simulated for 1 h, and the particle surface coverage distribution was estimated using a statistical approach for both an unstabilized prismatic spouted bed and one stabilized by draft plates.

Introduction

Spouted bed technology dates back to Mathur and Gishler (1955), who first applied it to the problem of drying wheat grains that were too coarse and aspherical to be treated in regular fluidized beds. Today, the technology has expanded to regular use in diverse areas including chemical vapour deposition on fine metal powders (Caussat, Juarez, & Vahlas, 2006) and high-density nuclear fuel pellets (Liu et al., 2017; Mollick et al., 2015; Marshall, 2017), spray coating of various materials such as fertilizers (da Rosa & dos Santos Rocha, 2010), coating of aerogel particles (Antonyuk, Heinrich, & Smirnova, 2012; Plawsky, Littman, & Paccione, 2010), spray granulation of composite materials (Wolff, Salikov, Antonyuk, Heinrich, & Schneider, 2014; Eichner, Salikov, Bassen, Heinrich, & Schneider, 2017), and combustion/pyrolysis (Alvarez, Amutio, Lopez, Bilbao, & Olazar, 2015; Ochoa et al., 2017; Alvarez et al., 2017).

Although these processes are commonly the domain of fluidized beds, spouted beds offer higher stability when using difficult-to-fluidize materials such as Geldart D particles or aspherical particles such as grains. This robustness is attributed to the unique bed distribution and circular flow structure within the apparatus. The gas is introduced in the middle of the apparatus and accelerates particles vertically from the surrounding particle bulk, creating the titular spout. As the gas jet diffuses above the surface of the particle bulk, entrained particles decelerate and fall down onto the bulk, which is commonly called the annulus. The annulus rests on slanted walls, causing the particles to flow towards the bulk. This explanation is idealistic, as the flow pattern of real apparatuses deviates from this pattern depending on the operating regime. The apparatuses can be constructed either asymmetrically, axisymmetrically/conically, or prismatically/slot-rectangularly (Piskova & Mörl, 2008). The first spouted beds were conical designs and were typically operated using high bed heights. The prismatic type has found commercial adoption (Jacob, 2009) because of the advantage of easy scale-up by extrusion of the process chamber and is commonly operated at shallow bed levels to ensure intense mixing and phase interaction. For these prismatic spouted beds, research is typically conducted using pseudo-2D replica of commercial apparatuses to reduce system complexity and enable computational modelling.

* Corresponding author.
E-mail address: paul.kieckhefen@tuhh.de (P. Kieckhefen).

https://doi.org/10.1016/j.partic.2018.01.008

Nomenclature

Greek symbols

$\delta\alpha$	Excess phase volume fraction
α	Phase volume fraction
η	Efficiency
ε	Poisson's ratio
γ	Arbitrary field
λ	Filter coefficient
ν	Kinematic viscosity, m^2/s
φ	Surface fraction
ρ	Density, kg/m^3
τ	Residence time, s
$\boldsymbol{\tau}$	Deviatoric stress tensor, N/m^2
$\boldsymbol{\omega}$	Angular velocity, s^{-1}

Latin symbols

A	Model parameter (Kolakaluri model)
d	Diameter, m
D_0	Diffusion coefficient, m^2/s
f	Fraction of particle surface coated by a single droplet
$\mathbf{F}$	Force, N
$\mathbf{g}$	Gravitational acceleration, m/s^2
J	Moment of inertia, kg/m^2
m	Mass per volume kg/m^3
M	Mass, kg
N	Number
p	Pressure, Pa
$\mathbf{n}$	Normal vector
t	Time, s
Δt	Time step, s

Symbol

$\mathbf{T}$	Torque, N m
$\mathbf{u}$	Phase velocity, m/s
V	Volume, m^3
Δx	Width/length, m
$\mathbf{x}$	Coordinate, m
Y	Young's modulus, Pa

Dimensionless numbers

Co	Courant number
Re	Reynolds number
St	Stokes number

Subscripts/superscripts

coll	Collected
dep	Deposition
D	Droplet/spray phase
eff	Effective
fluc	Fluctuation
fr	Friction
G	Gas phase
min	Minimum
n	Normal
P	Particle phase
rec	Recurrence field/quantity
rfr	Rolling friction
t	Tangential
W	Apparatus wall

Abbreviations

CFD	Computational fluid dynamics
DEM	Discrete element method
rCFD	Recurrence CFD

Gryczka et al. (2008) characterized the pneumatic behaviour of one such prismatic pseudo-2D apparatus, and Salikov et al. (2015) created a regime map for Geldart D particles. They observed that with increasing gas velocity, the pressure drop increases with bubbling occurring at a certain point. At the minimum spouting velocity, the pressure drop decreases and spouting is initiated. With increasing gas flow rate, the bed expands further into the process chamber and instabilities such as lateral spout deflections occur. The pressure drop oscillates regularly in the dense spouting regime and becomes more irregular with increasing gas velocity while the fluctuation intensity decreases and the primary frequency increases. These oscillations are caused by the spout–annulus interactions, as the annulus flowing into the spout region causes particle acceleration as well as an initial increase in the pressure drop followed by a subsequent decrease as the particles are cleared from the region. Instabilities arise because of the higher bed expansions, as these equate to a lower annulus height with less bulk solid load stabilizing the spout, preventing self-amplifying deflection and lateral bed distribution asymmetry. At very high flow rates, the pressure drop fluctuations disappear because of the homogeneous distribution of the bed in the process chamber and the lack of an annulus to cause fluctuations. This flow regime is called dilute spouting.

Spouted beds are well suited for spray coating because of the intense heat and mass transfer between the gas and particle phase (Kucharski & Kmiec, 1983). De Oliveira, Freire, and Coury (1997) used a cylindrical–conical spouted bed to coat alumina particles with a sucrose solution with high homogeneity and observed that the hydrodynamic operating regime had a substantial effect on particle growth.

Most previous works have applied the fully Eulerian two-fluid model (TFM) or the Eulerian–Lagrangian computational fluid dynamics–discrete element method (CFD–DEM) to spouted beds. Both methods have advantages and disadvantages depending on the context. The TFM uses the kinetic theory of granular flow, as described by Lun, Savage, Jeffrey, and Chepurniy (1984), and models granular motion in an Eulerian frame of reference using the concept of granular temperature and closures for frictional and normal stresses. This approach enables the efficient treatment of systems encompassing billions of very fine particles, as the computational demand scales with the number of grid cells instead of the number of individual particles. There are constraints on the cell size as coarse grids may not resolve all relevant flow structures and thus introduce inaccuracies (Schneiderbauer & Pirker, 2014). Gryczka et al. (2009) and Jacob (2009) conducted various TFM studies on a pseudo-2D spouted bed using Fluent and were unsuccessful in reproducing the pressure drop fluctuations.

Unresolved CFD–DEM, as elaborated in the work of Zhu, Zhou, Yang, and Yu (2007), uses an Eulerian description of the fluid flow and tracks the solid phase using computational parcels, which represent the motion of individual physical particles, or multitudes for coarse-graining (Bierwisch, Kraft, Riedel, and Moseler, 2009). Parcel contacts are commonly resolved using a soft-sphere approach, in which parcels are allowed to overlap and time steps on the order of 10^{-6} s are required by the contact model. Volume fractions are mapped to an Eulerian grid, where the flow is solved. Drag closures place a constraint on the cell size, as they model the effect of unresolved flow features such as swarming to a certain extent. A comprehensive treatment of the grid sensitivity of CFD–DEM can be found in the work of Radl and Sundaresan (2014). The main computational demand lies in the resolution of interparticle contacts. Although this approach allows for the accurate depiction of bulk solid motion, industrial and even pilot-scale systems commonly contain too many parcels for simulation without the application of coarse graining (Nasato, Goniva, Pirker, & Kloss, 2015). Salikov et al. (2015) conducted CFD–DEM simulations of pseudo-2D spouted

beds in stable and unstable regimes and found excellent agreement of the pressure drop fluctuation. Pietsch et al. (2017) extended this work to Geldart B particles using coarse-graining in 3D spouted beds. These works only simulated tens of seconds of operation, whereas spray coating requires on the order of tens of minutes for completion under experimental conditions.

In a seminal paper (Lichtenegger & Pirker, 2016), some of the current authors proposed the time extrapolation of recurrent flows by first conducting fully resolved simulations, storing the flow fields, and subsequently scoring the pairwise similarity of system states in the form of a recurrence plot (Eckmann, Kamphorst, & Ruelle, 1987). For the extrapolation, intervals of contiguous flow field states are alternated with random jumps to recreate the pseudo-periodic nature of the system while describing the transport of passive scalars. This task can be achieved by solving either Eulerian transport equations or transporting Lagrangian tracers.

The concept was first tested on a bubble column simulated using TFM and a steelmaking converter simulated using the volume-of-fluid approach. Although the bubble column showed superior performance when the Eulerian rCFD approach was applied, the steelmaking converter benefited from Lagrangian treatment. Some of the current authors applied the Lagrangian variant to a fluidized bed (Lichtenegger & Pirker, 2017; Lichtenegger, Peters, Kuipers, & Pirker, 2017) and extended the method to predict heat transfer; the results (extrapolated from a few seconds of data) showed excellent agreement of the bed distribution reproduction and global heat transfer characteristics on the scale of minute, extrapolated from few seconds of data.

In this work, we applied the Lagrangian rCFD method to a three-dimensional spouted bed simulated using CFD–DEM, paralleling the previous works conducted by some of the current authors (Pietsch et al., 2017). We first validated the method by assessing the reproduction of particle volume fractions and the prediction of particle holdups and residence times in a fictitious spray zone. Based on this preliminary work, longer (1 h ≡ 3600 s) spray-injection simulations were used to study the coating quality in a three-dimensional laboratory-scale spouted bed equipped with and without draft plates.

Simulations

CFD–DEM simulation

As we will only provide a short overview of the CFD–DEM method, the reader is referred to the work of Zhou, Kuang, Chu, and Yu (2010) for an in-depth theoretical treatment and to the work of Kloss, Goniva, Hager, Amberger, and Pirker (2012) for implementation of this method in the CFDEMcoupling software.

Gas-phase governing equations

The gas phase was assumed to behave as an incompressible fluid at the low velocities involved. Its time evolution was modelled in an Eulerian frame of reference using the continuum Eq. (1) and momentum transport Eq. (2)

$$\frac{\partial \alpha_G}{\partial t} + \nabla \cdot (\alpha_G \mathbf{u}_G) = 0, \tag{1}$$

$$\frac{\partial (\alpha_G \mathbf{u}_G)}{\partial t} + \nabla \cdot \alpha_G \mathbf{u}_G \mathbf{u}_G = -\alpha_G \frac{\nabla p}{\rho_G} + \alpha_G \frac{\nabla \cdot \boldsymbol{\tau}_G}{\rho_G} + \alpha_G \frac{\sum_i \mathbf{F}_{i,\mathrm{drag}}}{\rho_G V}, \tag{2}$$

where u_G, α_G, and ρ_G are the velocity, volume fraction, and density of the gas phase, respectively; p is the pressure; and V is the volume of the corresponding mesh cell. Under the assumption of Newtonian fluid behaviour, the deviatoric stress tensor is given by $\boldsymbol{\tau}_G = \rho_G \nu_G \left(\nabla \mathbf{u}_G + (\nabla \mathbf{u}_G)^{\dagger}\right)$. The net interphase force acting upon a particle i is given by $\mathbf{F}_{i,\mathrm{interphase}} = \mathbf{F}_{i,\mathrm{drag}} + \mathbf{F}_{i,\mathrm{p}}$, where $\mathbf{F}_{i,\mathrm{p}} = V_i \nabla p$ is the pressure gradient force. The drag force $\mathbf{F}_{i,\mathrm{drag}}$ was calculated using the correlation developed by Beetstra, van der Hoef, and Kuipers (2007).

Because of the fine mesh in the inlet region, the solid phase volume fraction was calculated by dividing each particle into 29 points and mapping these points to the mesh. Details of this procedure can be found in Radl, Gonzales, Goniva, and Pirker (2014). The volume fraction field and momentum exchange field were smoothened using an approach developed by Pirker, Kahrimanovic, and Goniva (2011) to ensure stability and enable the use of higher time steps. For a field γ that is to be smoothened, a conservative diffusion equation

$$\frac{\partial \gamma}{\partial t} = \frac{L^2_{\mathrm{smooth}}}{\Delta t_{\mathrm{CFD}}} \nabla^2 \gamma, \tag{3}$$

is solved (Radl et al., 2014), where L_{smooth} is the smoothing length, which is commonly selected to be on the order of three particle diameters.

Particle equations of motion

In DEM, as proposed by Cundall and Strack (1979) and implemented in LIGGGHTS (Kloss et al., 2012), particle motion is resolved by solving the Newtonian equations of motion

$$\ddot{\mathbf{x}}_i = \frac{1}{M_i} \left(\sum_j \mathbf{F}_{j \to i} + \mathbf{F}_{i,\mathrm{interphase}} \right) + \mathbf{g}, \tag{4}$$

$$\dot{\boldsymbol{\omega}}_i = \frac{1}{J_i} \sum_j \mathbf{T}_{j \to i}, \tag{5}$$

where $\mathbf{x}_i$ and M_i are the position and mass of a particle i, respectively; $\mathbf{g}$ is the gravitational acceleration vector; $\boldsymbol{\omega}$ is the angular velocity; J_i the moment of inertia; and $\mathbf{T}_{j \to i}$ is the torque acting on i due to j. The interparticle contact force $\mathbf{F}_{j \to i} = \mathbf{F}^{\mathrm{n}}_{j \to i} + \mathbf{F}^{\mathrm{t}}_{j \to i}$ of particle j acting upon another particle i is composed of a normal component $\mathbf{F}^{\mathrm{n}}_{j \to i}$ and a tangential component $\mathbf{F}^{\mathrm{t}}_{j \to i}$. The soft-sphere model, as implemented in LIGGGHTS, uses a global time step and integrates over all forces acting upon the particles. Contact forces are resolved by allowing the particles to overlap and by applying overlap-dependent force models such as the Hertz–Mindlin–Tsuji model (Tsuji, Tanaka, & Ishida, 1992). These models account for the single-particle mechanical properties such as the coefficient of restitution, modulus of elasticity, and Poisson's ratio. The maximum particle overlap should be kept under 0.3% of the particle radius (Lommen, Schott, & Lodewijks, 2014) for accurate reproduction of bulk behaviour, which puts restraints on the value of the global time step. Rolling friction was modelled using the constant directional torque model as described in the work of Ai, Chen, Rotter, and Ooi (2011), in which a torque proportional to the difference in angular velocity of two interacting particles was applied.

Recurrence CFD simulations

As previously proposed by some of the current authors (Lichtenegger & Pirker, 2016), the recurrent nature of certain flows can be used to time-extrapolate these processes using tools from recurrence statistics, namely recurrence plots and signal reconstruction. We will only provide a brief summary of the aspects of the method that pertain to the current case.

Recurrence statistics

As described in Lichtenegger et al. (2017), the continuous recurrence plot R_{α_G} is constructed using the gas phase volume fraction α_G:

$$R_{\alpha_G}(t_i, t_j) = 1 - \frac{1}{N_{\alpha_G}} \int_V (\alpha_G(t_i) - \alpha_G(t_j))^2 \, dV, \tag{6}$$

$$N_{\alpha_G} = \max_{t_i, t_j} \int_V (\alpha_G(t_i) - \alpha_G(t_j))^2 \, dV, \tag{7}$$

where t_i and t_j are two times with corresponding flow states, V is the entirety of the flow domain, and N_{α_G} is a normalization factor. Because of the normalization, the main diagonal contains values of 1 and the most dissimilar states have values of 0.

The temporal resolution needed for recurrent pattern reconstruction is limited by the temporal requirement

$$\Delta t_{\text{rec}} < \sqrt{\frac{\langle \gamma^2 \rangle}{\langle \dot{\gamma}^2 \rangle}}, \tag{8}$$

for a given field quantity γ, where $\langle \cdot \rangle$ denotes time averaging. The field-sampling interval Δt_{rec} was selected to satisfy these requirements.

Previous experimental work on spouted beds by Wang, Zhong, and Jiaqiang (2012) applied the original, binary recurrence plot method (Eckmann et al., 1987) to attractors reconstructed from the time delay embedded from the pressure drop time and successfully detected recurrent patterns specific to certain flow regimes in spouted beds.

Recurrent processes

Based on the recurrence plot and underlying field data, the recurrent flow patterns can be extrapolated by constructing a sequence of time indices that correspond to fields in the sampled database. Practically, this task is realized by separating the sampled field database into two halves. If the current sequence of consecutive fields ends in the second half of the database, a search for the maximum in similarity is performed in the first half, or vice versa, and this maximum is used as a starting point for the next sequence. In the remainder of this paper, we will refer to such fields as "recurrence fields".

Lagrangian rCFD

For each step within a sequence, the corresponding gas phase velocity $\mathbf{u}_G^{\text{rec}}$, particle phase velocity $\mathbf{u}_P^{\text{rec}}$, and particle volume fraction α_P^{rec} fields are loaded from the database. Based on these velocities, tracers are evolved by integrating

$$\dot{\mathbf{x}}_i = \mathbf{u}_P^{\text{rec}} + \mathbf{u}_{\text{fluc}}, \tag{9}$$

where $\mathbf{u}_P^{\text{rec}}$ is the particle phase velocity interpolated on the recurrence field and $\mathbf{u}_{\text{fluc}}$ is the fluctuation velocity. This additional velocity component is introduced to model the effect of interparticle collisions and to effectively prevent overpacking of tracers relative to the recurrence phase fractions. An expression for this component was derived by Lichtenegger and Pirker (2016) from first principles inspired by classical Brownian diffusion:

$$\mathbf{u}_{\text{fluc}} = \mathbf{n}_{\text{rand}} \sqrt{D_0 \frac{\delta\alpha_P}{6\pi \Delta t \alpha_P}}, \tag{10}$$

where $\mathbf{n}_{\text{rand}}$ is a random unit vector with $\|\mathbf{n}_{\text{rand}}\| = 1$, D_0 is the diffusion coefficient, $\delta\alpha_P = \max(0, \alpha_P - \alpha_P^{\text{rec}})$ is the excess volume fraction, and Δt is the local time step. The selection of D_0 is highly dependent on the flow situation because of its purpose in modelling granular temperature/collisions, and as such, D_0 must be calibrated with respect to the underlying CFD–DEM simulation. For tracers in regions with no recurrence information, as qualified by $\alpha_P^{\text{rec}} < 0.02$, the trajectory was calculated according to the effect of single-sphere drag force and gravity.

Spray modelling

The injected spray was modelled as Lagrangian droplet parcels with mass $M_D N_D$ with N_D droplets in a parcel. Because of their small diameter and low relaxation time $t_{\text{relax,D}} = \rho_D d_D^2/(18\nu_G\rho_G) < 5$ ms, the droplets were assumed to move at the fluid velocity, which avoids the need for calculation of the drag force. The droplets were injected at the nozzle inlet patch, which was angled to reproduce the experimentally measured spray cone, as outlined in our previous work (Pietsch et al., 2018). In addition, we assumed no droplet evaporation, and droplet parcels were removed from the system when they contacted the apparatus walls or outlet.

The droplet deposition was modelled using a filter correlation proposed by Kolakaluri (2013) to avoid numerically expensive direct contact detection. The target quantity was the deposition efficiency

$$\eta_{\text{dep}} = 1.5\lambda \Delta t_{\text{rCFD}} \|\mathbf{u}_{\text{G,rec}} - \mathbf{u}_{\text{P,rec}}\| \alpha_P / d_P, \tag{11}$$

within a single time step, according to which mass is stripped from the droplet parcels. A similar approach was used by Askarishahi, Salehi, and Radl (2017), albeit using an Eulerian droplet phase. The filter coefficient,

$$\lambda = \frac{\text{St}_{\text{eff}}^{3.2}}{\text{St}_{\text{eff}}^{3.2} + 4.3}, \tag{12}$$

depends on the effective Stokes number

$$\text{St}_{\text{eff}} = \frac{\text{St}}{2}(A + 1.14\text{Re}_m^{1/5}\alpha_G^{-3/2}), \tag{13}$$

and the model parameter

$$A = \frac{6 - 6\alpha_P^{5/3}}{6 - 9\alpha_P^{1/3} + 9\alpha_P^{5/3} - 6\alpha_P^2}, \tag{14}$$

where $Re_m = (1-\alpha_P)\|\mathbf{u}_{\text{G,rec}} - \mathbf{u}_{\text{P,rec}}\| d_P/\nu_G$ is the superficial Reynolds number and $St = \|\mathbf{u}_G - \mathbf{u}_P\| d_D^2 \rho_P/(9 d_P \nu_G)$ is the Stokes number.

In every time step, the mass stripped from each droplet parcel is calculated, mapped onto an Eulerian field, and then distributed among the tracers in the cells. This process strips droplets from the droplet parcel until they are removed when $N_D < N_{D,\min} = 1$.

Droplet impacts coat the particle surface. Kariuki, Freireich, Smith, Rhodes, and Hapgood (2013) proposed using a statistical approach to calculate the percentage of a particle surface coated by impacting droplets. The key parameters in this approach are the area coated by a single droplet $A_{D,\text{proj}}$ and the ratio of this area to the total particle surface $f = \frac{A_{D,\text{proj}}}{A_P} = (\frac{d_D}{2d_P})^2$. The degree of coating can thus be approximated as

$$\varphi_{\text{coverage}} = 1 - (1-f)^{N_{\text{coll}}}, \tag{15}$$

where N_{coll} is the number of droplets collected by a particle. Although this approach does not consider spreading due to surface wetting, porosity, fluid flow, and particle rotation, it is effective in representing the general character of coating quality estimation, namely asymptotic behaviour regarding injection of more coating liquid.

Furthermore, we assume that the coating process has a negligible effect on the granular dynamics because of the low mass injected and general resistance of spouted beds to changing bed loads. The evaporation of the coating liquid is assumed to be instantaneous and to have no effect on the fluid dynamics, which is reasonable given the low injection rate and high gas flow rates,

Table 1
Process conditions and gas (subscript G) and droplet (subscript D) phase material properties.

Process conditions	
Process air flow rate, $\dot{V}_G$ (m^3/h)	230
Atomization air flow rate, $\dot{V}_{G,nozzle}$ (m^3/h)	5
Particle bed, M_P (kg)	1.5
Spray flow rate, $\dot{M}_{spray}$ (kg/h)	0.3
Gas phase properties	
Density, ρ_G (kg/m^3)	1.225
Kinematic viscosity, v_G (m^2/s)	1.5×10^{-5}
Droplet phase properties	
Droplet diameter, d_D (μm)	40
Droplet density, ρ_D (kg/m^3)	1000
Droplet injection rate, $\dot{N}_D$ (s^{-1})	1×10^5

Table 2
Mesh and numerical setup.

CFD mesh	
Number of mesh cells, N_{cells}	73,647
Cell sizes	
Inlet region, $\Delta x_{cells,in}$	2.5 mm ≈ $1.4d_P$
Process chamber, $\Delta x_{cells,pc}$	5 mm ≈ $2.8d_P$
Freeboard, $\Delta x_{cells,fb}$	10 mm ≈ $5.6d_P$
CFD–DEM simulation	
CFD time step, Δt_{CFD} (s)	2.5×10^{-5}
Maximum Courant number, $Co_{max,CFD}$	0.8
CFD write interval, $\Delta t_{W,CFD}$ (s)	5×10^{-3}
DEM time step, Δt_{DEM} (s)	1×10^{-6}
Number of particles, $N_{P,DEM}$	472,850
Recurrence CFD simulation	
Global time step, Δt_{rCFD} (s)	5×10^{-3}
Particle Courant number, $Co_{max,P,rCFD}$	1
Number of particle tracers, $N_{P,rCFD}$	472,850
Droplet parcel injection rate, $\dot{N}_{D,rCFD}$ (s^{-1})	1×10^5

equating to a maximum increase in the air humidity of approximately 1 g/kg.

Simulation setup

The process conditions and gas phase properties are listed in Table 1. The overall setup of the case was selected to be a scale-up of case 3 discussed by Salikov et al. (2015).

Geometry and mesh generation

The geometry of the apparatus is identical to that of the commercial ProCell 5 (Glatt GmbH, Germany) lab-scale spouted bed with a prismatic angle of 60°, width of 250 mm, and depth of 200 mm, similar to those used by Salikov et al. (2015), Gryczka et al. (2009), and Pietsch et al. (2017). The precise dimensions of the inlet geometry can be found in Gryczka et al. (2009). The lower region of the inlet geometry was simplified by removing the curved region and merging the two inlet slits.

The spray cone half-angle was experimentally determined to be approximately 17°. To reproduce the spray cone and its flow velocity profile, the boundary of the nozzle was curved to reproduce the complementary angle of 73°. Meshing was performed using the OpenFOAM hexahedral cut-cell mesher snappyHexMesh. The cell side lengths are listed in Table 2, and the resulting mesh is shown in Fig. 1. The particle (subscript P) and apparatus (subscript W) material and contact properties are listed in Table 3, which are adapted from Salikov et al. (2015).

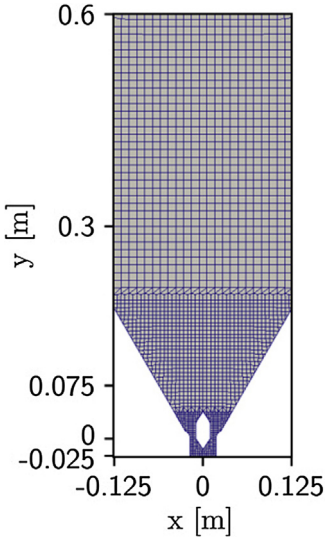

Fig. 1. Surface mesh of the apparatus.

Table 3
Particle (subscript P) and apparatus (subscript W) material and contact properties, adapted from Salikov et al. (2015).

Diameter, d_P (mm)		1.8
Particle density, ρ_P (kg/m^3)		1040
Young's modulus, $Y_P = Y_W$ (Pa)		1×10^9
Poisson's ratio, $\varepsilon_P = \varepsilon_W$		0.25
Coefficient of restitution	e_{P-P}	0.9
	e_{P-W}	0.75
Coefficient of friction	$k_{fr,P-P}$	0.5
	$k_{fr,P-W}$	0.24
Coefficient of rolling friction	$k_{rfr,P-P}$	0.06
	$k_{rfr,P-W}$	0.05

CFD–DEM simulations

The full simulations were conducted using an extended version of the CFDEMcoupling (Kloss et al., 2012) software package.

An overview of the numerical setup is provided in Table 2. The CFD time step Δt_{CFD} was set to satisfy $Co = u\Delta t/\Delta x < 1$ and did not exceed $\max(Co) \approx 0.8$ during the entire simulation. For the DEM part, the time step was set to be approximately 20% of the Rayleigh time. Interphase coupling was performed once per CFD time step, or every 25 DEM time steps. The smoothing length was set to 5×10^{-3} mm. The inlet was prescribed a fixed velocity boundary condition. For turbulence modelling, the k–ε model was used with an inlet turbulence intensity of 5%.

First, 1.5 kg of 1.8 mm γ-Al_2O_3 particles were inserted at a height of 0.2 m < y < 0.3 m within the freeboard region of the apparatus. The simulation was stopped after 3 s and resumed using a field sampling frequency of 200 Hz for 10 s, resulting in a field database comprising 2000 entries and requiring 16 GB of memory. The data generated in this run was not used for residence time computation to avoid biases. The simulation was continued for another 10 s, and the residence time within the cone, shown in Fig. 2, was calculated.

Another CFD–DEM simulation was performed using identical settings and geometry but featuring draft plates, as proposed by Pietsch et al. (2017). These draft plates were 60-mm high, located 10 mm above the mid profile, and distanced 45-mm apart.

rCFD simulations

The tracer equations of motion described in Eq. (9) were implemented based on the hard-sphere Lagrangian particle tracking (LPT) algorithm present in OpenFOAM 5.x (Weller, Tabor, Jasak,

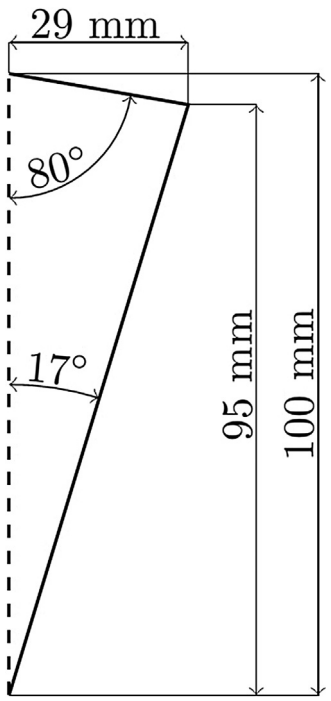

Fig. 2. Shape and dimensions of the spray cone used in both full CFD–DEM and rCFD simulations.

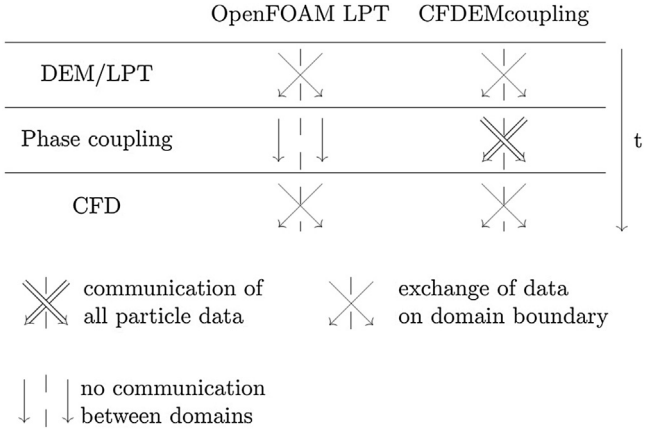

Fig. 3. Schematic of interprocess communication in CFDEMcoupling and OpenFOAM Lagrangian particle tracking (LPT).

& Fureby, 1998), which is described in detail in Macpherson, Nordin, and Weller (2010). This implementation enabled efficient treatment of the complex walls present in the geometry. For the walls, simple elastic restitution was assumed, unlike in our first implementation of this method in CFDEMcoupling using CFDEM/LIGGGHTS. There, simple reflective wall boundary conditions were applied to avoid costly contact detection.

Another notable difference is the mode of parallelization, as illustrated in Fig. 3. CFDEMcoupling uses different domain subdivisions for the CFD and DEM sides, which enables efficient dynamic load balancing on the DEM side but introduces a bottleneck: during coupling, the DEM information is distributed to all CFD processes, which is commonly called "all-to-all" communication and which can be very costly depending on the number of partitions and particles. Additionally, data must be copied between the constituent codes OpenFOAM and LIGGGHTS. In contrast, OpenFOAM LPT uses the same geometric subdivisions for both particles and the fluid domain, meaning that no further inter-process communication

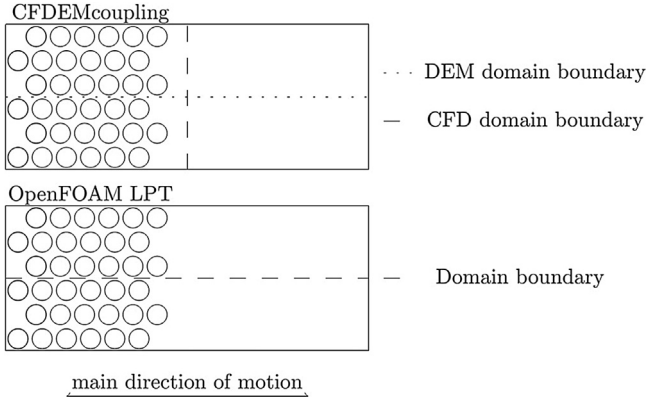

Fig. 4. Optimal domain decompositions using CFDEMcoupling employing "all-to-all" communication and OpenFOAM Lagrangian particle tracking (LPT).

needs to occur while evolving the particle cloud, except for interprocess boundary crossing of particles. This process requires careful selection of the domain decomposition geometry to ensure optimal performance for cases in which both CFD and DEM are similarly demanding; however, the Lagrangian phase is not homogeneously distributed, as illustrated for a simple case in Fig. 4. This problem does not appear for most Lagrangian rCFD applications, as the decomposition can be selected to represent a homogeneous distribution of particles among domains. The main computational demand here lies in the Euler–Lagrange mapping and solving the underlying physics such as transport processes and integration of equations of motion. These two steps benefit the most from a co-location of CFD field data and particle information within the same process, making OpenFOAM LPT the superior choice.

Short recurrence CFD simulations of 35 s were performed for the diffusion coefficient calibration using a sampling frequency of 200 Hz for the probes and 1 Hz for the fields. The fluctuation velocities were limited to 1 m/s to prevent tracers from diffusing farther than approximately one cell diameter in the process chamber within one time step. The first 5 s were not used for residence time calculation.

Results and discussion

CFD–DEM simulation

The vertical particle velocity as a function of time in prominent probing locations in the spout and annulus is shown in Fig. 5. The particles in the spout experienced mostly upwards motion, as expected. The maximum velocities here did not exceed 3 m/s with a root mean square (RMS) velocity of 1.2 m/s and a RMS temporal derivative of 28.2 m/s^2, giving an upper bound of the field sampling interval of $\Delta t_{w,CFD} < 0.04$ s. The particles in the annulus underwent alternating periods of upward and downward motion, indicating lateral spout ejections that are the defining feature of the instable operating regime. Notably, the low resulting RMS velocity and relatively high temporal variability resulted in a stricter criterion for the field sampling interval of $\Delta t_{w,CFD} < 0.02$ s. Therefore, a field sampling interval of $\Delta t_{w,CFD} = 0.005$ s was selected to ensure appropriate reproduction of the system dynamics. This interval was also assumed to be sufficient for the case containing draft plates, as these stabilize flow patterns in both the spout and annulus.

The resulting recurrence plot in Fig. 6 has many laminar diagonals, especially in the region $4\,\text{s} \leq t_{rec} \leq 8\,\text{s}$, indicating the presence of a high degree of recurrent system states within the sampled database as well as an interval with low recurrence within the sampled time span at $t_{rec} \approx 3$ s and $t_{rec} \approx 9$ s.

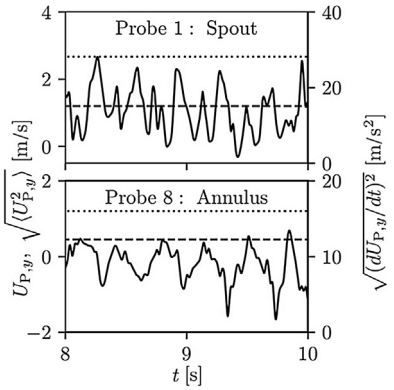

Fig. 5. Vertical particle velocities $U_{P,y}$ (straight line) at probe locations 1 (spout) and 8 (annulus) as well as the corresponding root mean square velocities $\sqrt{\langle U_{P,y}^2 \rangle}$ (dashed line) and temporal derivatives $\sqrt{\langle \left(dU_{P,y}/dt\right)^2 \rangle}$ (dotted line). The signals were low-pass filtered using a cut-off frequency of 50 Hz to remove numerical noise.

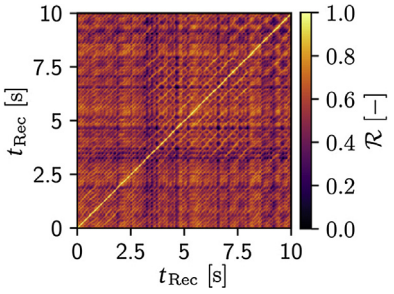

Fig. 6. Recurrence matrix derived from the volume fraction field α_P sampled for 10 s at 200 Hz.

Reproduction of bed distribution and dynamics in rCFD

To ensure the validity of the rCFD simulations and avoid overpacking of the tracer particles relative to the volume fractions present in the recurrence fields, the intensity of the velocity fluctuations was calibrated. For this process, 35-s simulations using diffusion coefficients in the range of $0 \leq D_0 \leq 1 \times 10^{-2}$ m^2/s were conducted. To eliminate the effect of random recurrence path calculation, a pre-calculated path was used for these simulations.

The success of the simulation can be judged by its ability to reproduce the instantaneous volume fractions at probe locations relative to the recurrence fields and the time-averaged volume fraction,as well as to predict the residence time within the previously described spray zone.

Reproduction of dynamic volume fraction

The resulting tracer volume fractions and corresponding recurrence particle volume fractions at a sample location in the spout region are plotted as a function of time in Fig. 7. Agreement of the recurrence particle volume fractions and tracer volume fractions implies accurate reproduction of both the bed distribution and granular fluxes, as for $D_0 \geq 5 \times 10^{-4}$ m^2/s, where an increase of the diffusion coefficient D_0 does not improve the agreement. For $D_0 < 1 \times 10^{-4}$ m^2/s, the tracer volume fraction frequently exceeded the recurrence volume fraction, which indicates inaccurate reproduction of the bed distribution. Here, the tracer volume fraction even exceeded the close-packed volume fraction limit of $\alpha_P > 0.67$. Without the relaxation model ($D_0 = 0$ m^2/s), the tracer volume fraction at the probing location was consistently lower than the recurrence volume fraction. This mismatch indicates that the bed distribution was severely misrepresented due to particles accumulating elsewhere in the system.

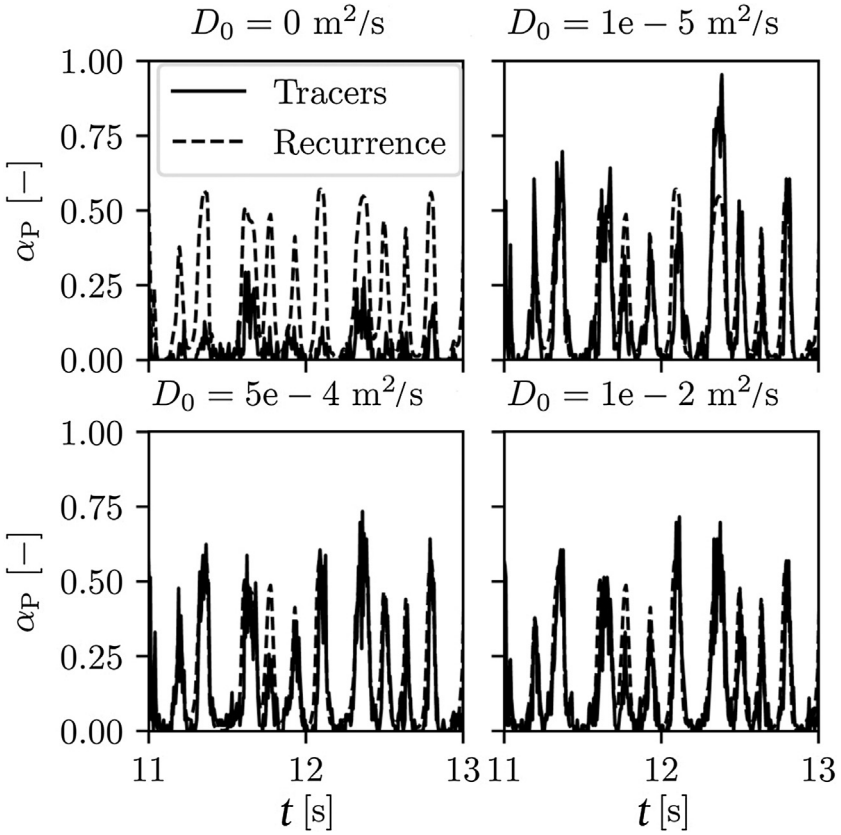

Fig. 7. Recurrence CFD tracer volume fractions for different diffusion coefficients D_0 and corresponding particle volume fractions at the probe location in the spout region at $x = 0$ m, $y = 0.075$ m, $z = 0.05$ m, which is approximately the same height and lateral positions as the fictitious spray zone.

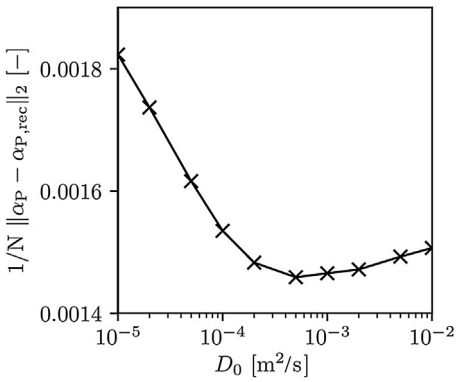

Fig. 8. Penalty scores for different diffusion coefficients.

To remove subjectivity from the selection of the diffusion coefficient, a penalty function $1/N_{\text{datapoints}} \|\alpha_P - \alpha_{P,rec}\|_2$ was applied to all 10 sampling locations in the apparatus. The locations were in prominent regions within the annulus and spout to enable the accuracy of the bed distribution reproduction to be gauged. The time-averaged penalty scores averaged over all locations for different diffusion coefficients are shown in Fig. 8. The penalty score decreased with increasing diffusion coefficient up to $D_0 = 1 \times 10^{-4}$ m²/s, at which point a minimum occurred. For higher diffusion coefficients, the score increased again, possibly due to artefacts induced by the strong diffusion. This behavior is generally in accordance with the qualitative observations made when comparing the tracer and recurrence volume fractions at a single sampling point.

Time-averaged volume fraction reproduction

Reproducing the time-averaged recurrence volume fraction determined by the tracers is a requirement for using the Lagrangian rCFD approach, as a failure to reproduce this parameter would invalidate all the results of further simulations. The resulting time-averaged tracer and recurrence volume fractions in a plane at $z = 0.1$ m are presented in Fig. 9. Applying no velocity fluctuations ($D_0 = 0$) resulted in very high, unphysical tracer volume fractions close to the walls and, consequently, lower bed concentrations and expansions in the spout regions. This problem persisted for low diffusion coefficients, e.g., $D_0 = 1 \times 10^{-5}$ m²/s. Starting with $D_0 = 5 \times 10^{-4}$ m²/s, the significantly overpacked regions in the annulus disappeared and the appropriate mean shape of the bulk was accurately reproduced. As higher diffusion coefficients introduce errors such as unphysical mixing in bulk regions, the lowest viable diffusion coefficient $D_0 = 5 \times 10^{-4}$ m²/s was selected for further investigations.

Influence on holdup and residence time distribution within a fictitious spray zone

To gauge the accuracy of the simulations relative to a real-world target value, a spray zone was defined. This step was valuable, as unlike the previous examples, the fate of single particles could be assessed, enabling clarification of the effect of random-walk-induced unphysical mixing.

Examples of the instantaneous spray zone holdup for different diffusion coefficients and the full CFD–DEM simulation are presented in Fig. 10. The signals have very similar pseudo-periodic patterns. Except for the simulation without the diffusion model, where poor distribution of solids led to an overall holdup underestimation, the peaks in the rCFD simulations were higher regardless of the diffusion coefficient. The mean holdup was generally only slightly overestimated relative to that of the full CFD–DEM simulation. These minor deviations may be explained by overpacking, indicating an insufficiency of the diffusion-based relaxation model.

The spray zone residence time distributions for various diffusion coefficients and for the full simulation are given in Fig. 11. As in the previous cases, a lack of diffusive relaxation leads to poor agreement with the CFD–DEM simulation. The use of higher diffusion coefficients resulted in good agreement with the CFD–DEM

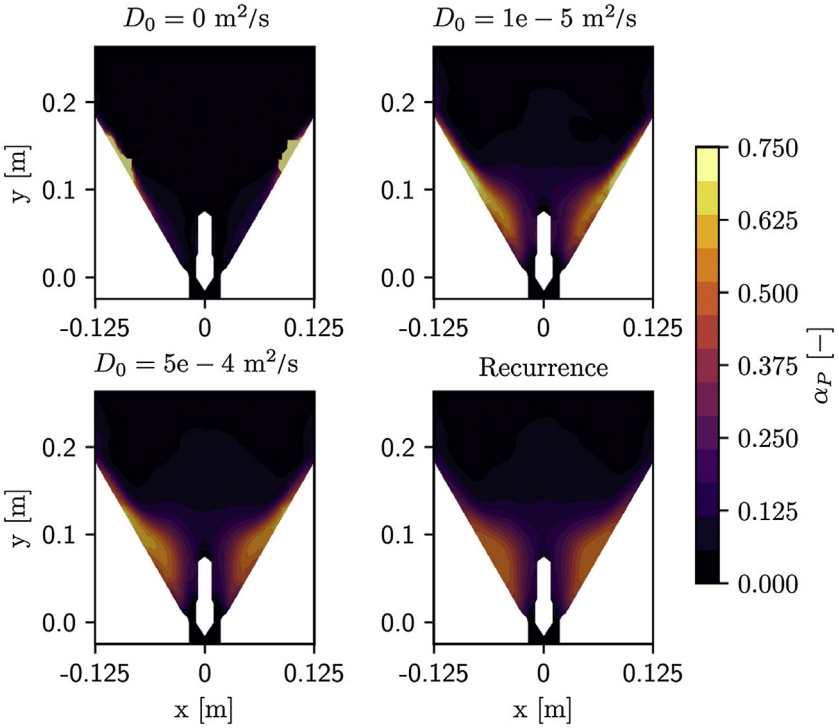

Fig. 9. Time-averaged particle volume fractions at $z = 0.1$ m. The plots titled "D_0" present the averaged tracer volume fractions for various diffusion coefficients and that titled "Recurrence" presents the time-averaged recurrence volume fraction field.

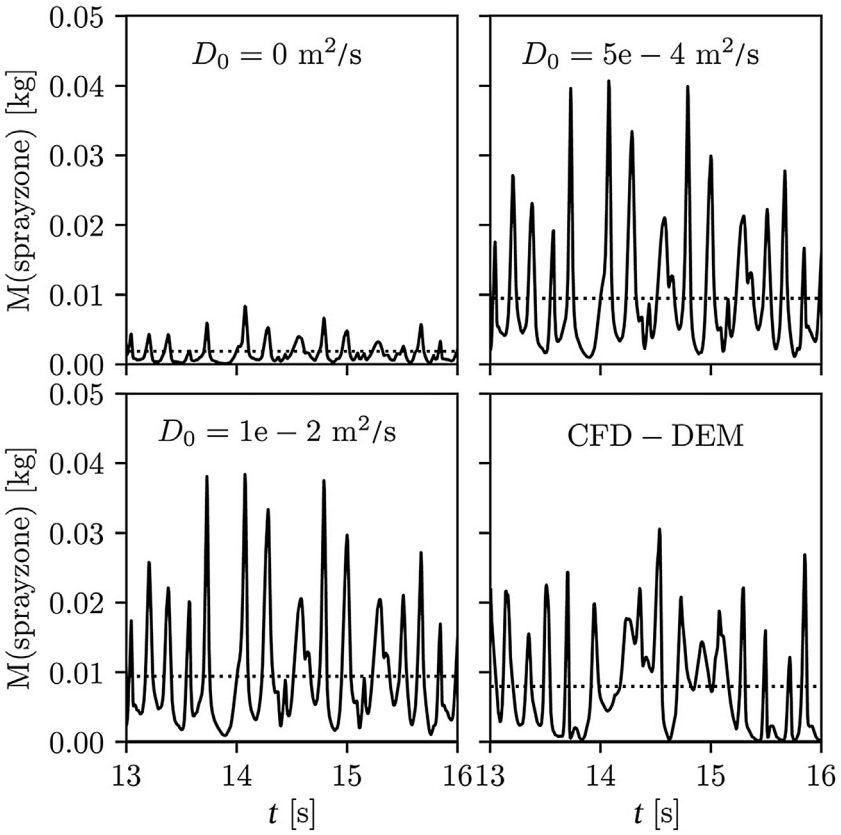

Fig. 10. Dependence of instantaneous spray cone holdup on diffusion coefficient for rCFD simulations and full CFD–DEM simulation. The dotted lines indicate the time-averaged holdups.

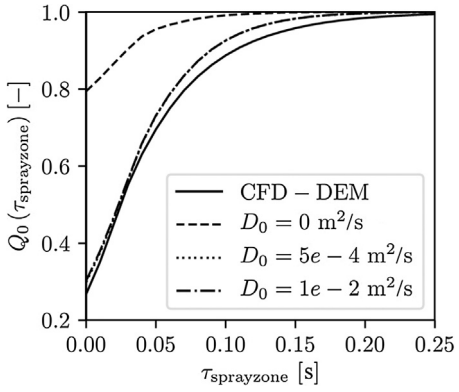

Fig. 11. Spray zone residence time distributions after 10-s simulation time for various diffusion coefficients. Note that the graphs for $D_0 = 5 \times 10^{-4}$ m^2/s (dotted) and $D_0 = 1 \times 10^{-2}$ m^2/s (dash-dot) practically overlap.

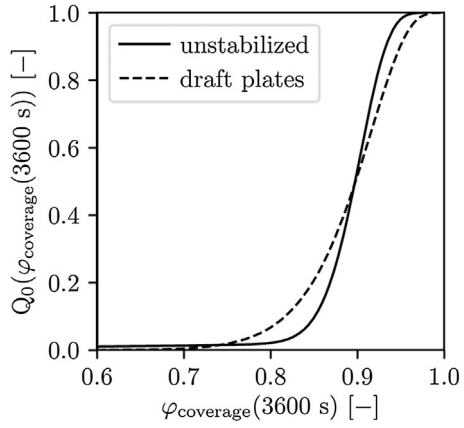

Fig. 12. Fractional surface coverage distributions after 1 h of spray injection.

simulation, with some underprediction of the fraction of particles with high residence times. As even excessive diffusion coefficients do not substantially affect the residence time distribution, it can be assumed that unphysical mixing does not occur to a degree that would adversely affect the outcome. The limit of the fluctuation velocity of 1 m/s might also play a role in preventing excessive diffusion.

Spray coating

The simulation predicted overspray of 2.3% for the unstabilised spouted bed and 0.8% for the stabilized one, which, while somewhat optimistic, qualitatively indicates that the process might benefit from the denser and less variable flow pattern in the stabilized apparatus.

The fractional surface coverage distributions calculated using Eq. (15) for the unstabilised spouted bed and that equipped with draft plates after 1 h of spray injection are shown in Fig. 12. Surprisingly, the median fractional coverage was identical at 90%, with an overall narrower distribution observed for the unstabilised system. This result can be attributed to inhibited mixing along the apparatus depth axis (z), as the primary component of particle motion is within the x–y plane. With the ejections suppressed by the draft plates, this mode of mixing is greatly reduced.

Based on these findings, characterization of the regions in which droplet deposition occurs was performed, as shown in Fig. 13. In the unstabilised apparatus, most deposition occurred directly above

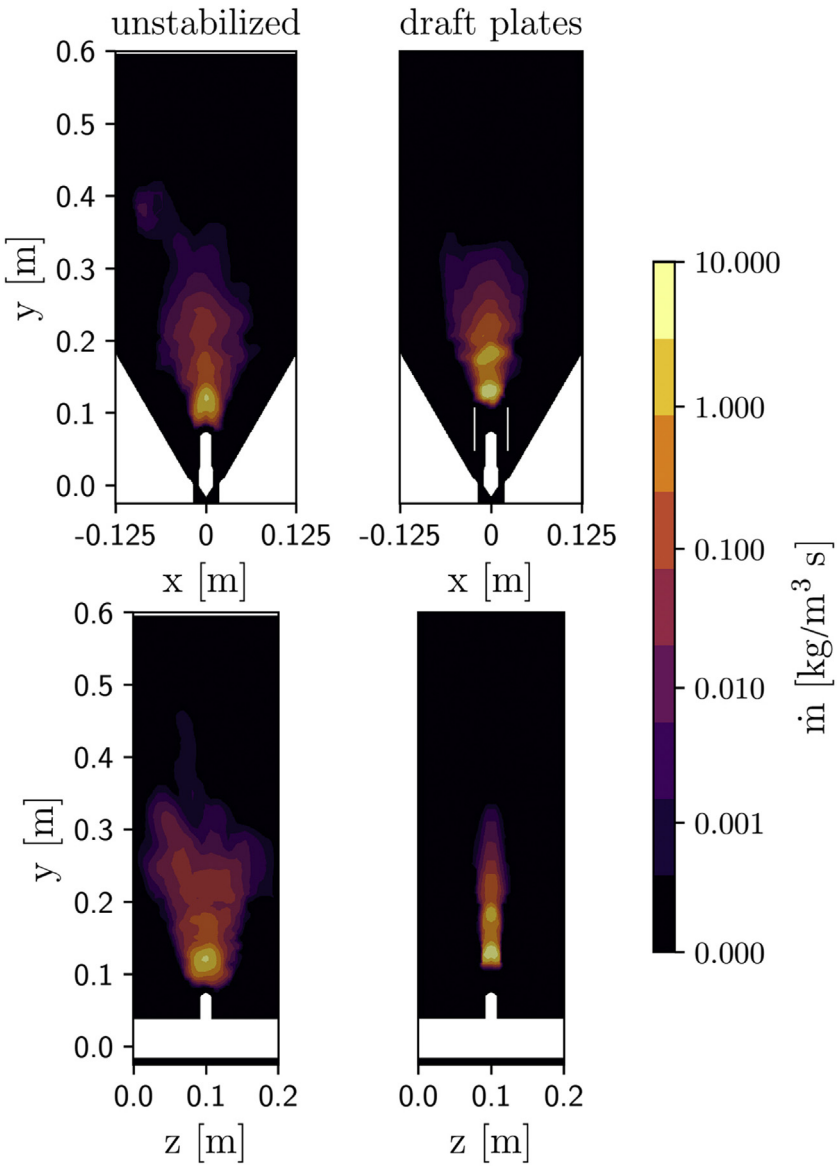

Fig. 13. Time-averaged deposition rate density distributions at the apparatus midplanes ($z = 0.1$ m in the upper plots and $x = 0$ m in the lower plots).

the nozzle within a diffuse cloud, which is in clear contrast to the apparatus with draft plates, for which the main deposition zone was more sharply defined and shifted approximately 2-cm higher to the upper end of the plates, possibly due to higher background gas velocities within the channel presented by the plates. Comparison of the lateral profiles indicated that the deposition area was very compact in its longitudinal expansion in the stabilized case, signifying less longitudinal gas flow, which could move either droplets or particles along this direction.

Overall, these findings provide insight into the optimization potential of the spouted bed apparatus. Although the evaluated design (Pietsch et al., 2017) did not improve the coating quality, it might be interesting for other applications. Processes requiring intensive contact with a granular catalyst should benefit from the increased stability, resulting in a narrow gas phase residence time distribution and low bypass; however, further investigation is required.

To reduce the calculation time without applying rCFD, one may be tempted to use time-averaged velocity and volume fraction fields to move tracers for both particles and droplets while modelling droplet deposition in the same way performed in this study. Although this approach may be viable for the stabilized apparatus, it would introduce great inaccuracies for the unstabilized variant, as any given state of the flow fields would differ greatly from the average because of the lateral deflections and irregular ejections.

Performance considerations

The CFD–DEM simulations required wall times of 13 days for 13-s simulations on 2×12 cores of Intel E5-2680v3 processors. The residence time calculations using rCFD were performed on 12 cores of the same hardware and required 36 min of wall time for 35 s, with 12 min spent loading the approximately 16 GB of recurrence fields from storage into memory and calculating the recurrence matrix. These parameters correspond to a 2100-fold net speedup when excluding the loading times, which become negligible when considering the overall duration of the simulations for which the application of rCFD is appropriate and desirable.

The spray simulations added the burden of another (negligible) set of recurrence tracers (spray parcels) and the droplet deposition calculations, which reduced the performance to ≈1500 s/day with a speedup of 1500 times. As the deposition algorithm only involves

one Eulerian field calculation and two non-nested loops over all tracers, this finding provided further evidence of the leanness and efficiency of the particle tracking algorithm present in OpenFOAM.

Discussion of model limitations

As promising as the findings and performance appear, the proposed method in its current state is only applicable to a specific class of processes. Recurrent flow patterns can be found on any scale in turbulent flow but are in practice modelled using a sub-grid-scale model. More complex physical models such as heat transfer or chemistry are usually solved using a steady-state solution of the system at hand or transient simulations for flows with strongly coupled physics for subsequent extrapolation in post-processing. Although rCFD can eliminate the need to extrapolate physics in post-processing by instead extrapolating the dynamics and directly solving the physics, it is only appropriate when negligible back-propagation from the solved physics to the fluid dynamics occurs.

A central weak point of the method in its current form is the relaxation mechanism. Although diffusion by random walk is a simple, inexpensive, and elegant solution to the overpacking problem, it also introduces artificial mixing. Here, a more sophisticated approach is needed that accounts for additional information about the state of the system during the recurrence database generation. For granular systems, appropriate quantities may be the granular temperature or statistical moments of the granular flux across cell faces.

Because the method trades time complexity for space complexity, memory usage will be one of the bottlenecks for application of the method to larger apparatuses. Using the method is only viable when recurrent patterns occur on time scales within a few orders of magnitude of the temporal resolution criterion (Eq. (8)), as otherwise, the memory requirements would be increased. The size of the recurrence database must be carefully balanced between the lower bound of containing all prominent flow patterns and the upper bound of the available memory size.

A case that would greatly benefit from the rCFD method is one exhibiting ideally strongly periodic patterns, which deviate strongly from the mean, as this would inhibit convergence of steady-state models and thus require computationally expensive transient simulations.

Conclusions

In this work, we successfully applied the rCFD method to a laboratory-scale 3D spouted bed apparatus. This effort presented a particular challenge, as the entire set of flow regimes, ranging from bulk flow in the annulus to dense and dilute flow in the spout and fountain, were represented. The method was shown to accurately reproduce flow patterns, as evident by a comparison of the resulting averaged volume fractions and residence time distribution within a spray cone with those obtained from a full CFD–DEM simulation, while requiring only 0.05% of the calculation time after generating the recurrence database.

This performance gain allowed for the direct investigation of spray injection on the time scale of 1 h in less than three days of wall time, which would have required a total of 3600 days using full CFD–DEM. The addition of draft plates led to worse mixing performance, which can be attributed to the stabilized spouting pattern, and produced a wider surface coverage distribution among the particles. This work is only a first step in exploring the potential of the apparatus and its modifications for practical applications. The reduced mixing along the apparatus depth may also introduce opportunities for continuous drying in apparatuses scaled up by increasing the apparatus depth or in chemical reactors where the granular phase acts as a catalyst.

In future works, rCFD will be applied to additional problems with diverse physical challenges, and, in particular, its limits must be systematically determined. New relaxation models should be developed using simpler dense granular and bulk flow situations because in more complex systems, inaccuracies may be masked by the interplay of different factors. Further developments regarding algorithmic reduction of sampled data will pave the way to broad application for industrial-scale problems. As for spouted beds, new approaches for measuring, or ideally monitoring, coating quality are needed and would provide a chance to validate the assumptions made and conclusions drawn in this work.

Acknowledgements

T. Lichtenegger acknowledges funding from the Linz Institute of Technology (LIT), Johannes Kepler University (project LIT-2016-1-YOU-007). S. Pietsch acknowledges financial support from BASF SE.

References

Ai, J., Chen, J. F., Rotter, J. M., & Ooi, J. Y. (2011). Assessment of rolling resistance models in discrete element simulations. *Powder Technology*, *206*(3), 269–282.
Alvarez, J., Amutio, M., Lopez, G., Bilbao, J., & Olazar, M. (2015). Fast co-pyrolysis of sewage sludge and lignocellulosic biomass in a conical spouted bed reactor. *Fuel*, *159*, 810–818.
Alvarez, J., Lopez, G., Amutio, M., Mkhize, N. M., Danon, B., van der Gryp, P., et al. (2017). Evaluation of the properties of tyre pyrolysis oils obtained in a conical spouted bed reactor. *Energy*, *128*, 463–474.
Antonyuk, S., Heinrich, S., & Smirnova, I. (2012). Discrete element study of aerogel particle dynamics in a spouted bed apparatus. *Chemical Engineering & Technology*, *35*(8), 1427–1434.
Askarishahi, M., Salehi, M. S., & Radl, S. (2017). Full-physics simulations of spray-particle interaction in a bubbling fluidized bed. *AIChE Journal*, *63*(7), 2569–2587.
Beetstra, R., van der Hoef, M. A., & Kuipers, J. A. M. (2007). Drag force of intermediate Reynolds number flow past mono-and bidisperse arrays of spheres. *AIChE Journal*, *53*(2), 489–501.
Bierwisch, C., Kraft, T., Riedel, H., & Moseler, M. (2009). Three-dimensional discrete element models for the granular statics and dynamics of powders in cavity filling. *Journal of the Mechanics and Physics of Solids*, *57*(1), 10–31.
Caussat, B., Juarez, F. L., & Vahlas, C. (2006). Hydrodynamic study of fine metallic powders in an original spouted bed contactor in view of chemical vapor deposition treatments. *Powder Technology*, *165*(2), 65–72.
Cundall, P. A., & Strack, O. D. L. (1979). A discrete numerical model for granular assemblies. *Géotechnique*, *29*(1), 47–65.
da Rosa, G. S., & dos Santos Rocha, S. C. (2010). Effect of process conditions on particle growth for spouted bed coating of urea. *Chemical Engineering and Processing: Process Intensification*, *49*(8), 836–842.
De Oliveira, W. P., Freire, J. T., & Coury, J. R. (1997). Analysis of particle coating by spouted bed process. *International Journal of Pharmaceutics*, *158*(1), 1–9.
Eckmann, J. P., Kamphorst, S. O., & Ruelle, D. (1987). Recurrence plots of dynamical systems. *Europhysics Letters*, *4*(9), 973–977.
Eichner, E., Salikov, V., Bassen, P., Heinrich, S., & Schneider, G. A. (2017). Using dilute spouting for fabrication of highly filled metal–polymer composite materials. *Powder Technology*, *316*, 426–433.
Gryczka, O., Heinrich, S., Deen, N. G., van Sint Annaland, M., Kuipers, J. A. M., Jacob, M., et al. (2009). Characterization and CFD-modeling of the hydrodynamics of a prismatic spouted bed apparatus. *Chemical Engineering Science*, *64*(14), 3352–3375.
Gryczka, O., Heinrich, S., Miteva, V., Deen, N. G., Kuipers, J. A. M., Jacob, M., et al. (2008). Characterization of the pneumatic behavior of a novel spouted bed apparatus with two adjustable gas inlets. *Chemical Engineering Science*, *63*(3), 791–814.
Jacob, M. (2009). ProCell technology: Modelling and application. *Powder Technology*, *189*(2), 332–342.
Kariuki, W. I., Freireich, B., Smith, R. M., Rhodes, M., & Hapgood, K. P. (2013). Distribution nucleation: Quantifying liquid distribution on the particle surface using the dimensionless particle coating number. *Chemical Engineering Science*, *92*, 134–145.
Kloss, C., Goniva, C., Hager, A., Amberger, S., & Pirker, S. (2012). Models, algorithms and validation for opensource DEM and CFD–DEM. *Progress in Computational Fluid Dynamics, An International Journal*, *12*(2–3), 140–152.
Kolakaluri, R. (2013). *Direct numerical simulations and analytical modeling of granular filtration. Doctoral dissertation*. USA: Iowa State University.
Kucharski, J., & Kmiec, A. (1983). Hydrodynamics, heat and mass transfer during coating of tablets in a spouted bed. *The Canadian Journal of Chemical Engineering*, *61*(3), 435–439.

Lichtenegger, T., Peters, E. A. J. F., Kuipers, J. A. M., & Pirker, S. (2017). A recurrence CFD study of heat transfer in a fluidized bed. *Chemical Engineering Science*, *172*, 310–322.

Lichtenegger, T., & Pirker, S. (2016). Recurrence CFD—A novel approach to simulate multiphase flows with strongly separated time scales. *Chemical Engineering Science*, *153*, 394–410.

Lichtenegger, T., & Pirker, S. (2017). Extremely fast simulations of heat transfer in fluidized beds. *12th international conference on CFD in oil & gas, metallurgical and process industries*, 47–51.

Liu, R., Liu, M., Shao, Y., Chen, X., Ma, J., & Liu, B. (2017). A novel coated-particle design and fluidized-bed chemical vapor deposition preparation method for fuel-element identification in a nuclear reactor. *Particuology*, *31*, 35–41.

Lommen, S., Schott, D., & Lodewijks, G. (2014). DEM speedup: Stiffness effects on behavior of bulk material. *Particuology*, *12*, 107–112.

Lun, C. K. K., Savage, S. B., Jeffrey, D. J., & Chepurniy, N. (1984). Kinetic theories for granular flow: Inelastic particles in Couette flow and slightly inelastic particles in a general flowfield. *Journal of Fluid Mechanics*, *140*, 223–256.

Marshall, D. W. (2017). Spouted bed design considerations for coated nuclear fuel particles. *Powder Technology*, *316*, 421–425.

Mathur, K. B., & Gishler, P. E. (1955). A technique for contacting gases with coarse solid particles. *AIChE Journal*, *1*(2), 157–164.

Mollick, P. K., Venugopalan, R., Roy, M., Rao, P. T., Sathiyamoorthy, D., Sengupta, P., et al. (2015). Deposition of diversely textured buffer pyrolytic carbon layer in TRISO coated particle by controlled manipulation of spouted bed hydrodynamics. *Chemical Engineering Science*, *128*, 44–53.

Nasato, D. S., Goniva, C., Pirker, S., & Kloss, C. (2015). Coarse graining for large-scale DEM simulations of particle flow—An investigation on contact and cohesion models. *Procedia Engineering*, *102*, 1484–1490.

Ochoa, A., Barbarias, I., Artetxe, M., Gayubo, A. G., Olazar, M., Bilbao, J., et al. (2017). Deactivation dynamics of a Ni supported catalyst during the steam reforming of volatiles from waste polyethylene pyrolysis. *Applied Catalysis B: Environmental*, *209*, 554–565.

Pietsch, S., Heinrich, S., Karpinski, K., Müller, M., Schönherr, M., & Jäger, F. K. (2017). CFD-DEM modeling of a three-dimensional prismatic spouted bed. *Powder Technology*, *316*, 245–255.

Pietsch, S., Kieckhefen, P., Heinrich, S., Müller, M., Schönherr, M., & Jäger, F. K. (2018). CFD-DEM modelling of circulation frequencies and residence times in a prismatic spouted bed. *Chemical Engineering Research and Design*, *132*, 1105–1116.

Pirker, S., Kahrimanovic, D., & Goniva, C. (2011). Improving the applicability of discrete phase simulations by smoothening their exchange fields. *Applied Mathematical Modelling*, *35*(5), 2479–2488.

Piskova, E., & Mörl, L. (2008). Characterization of spouted bed regimes using pressure fluctuation signals. *Chemical Engineering Science*, *63*(9), 2307–2316.

Plawsky, J. L., Littman, H., & Paccione, J. D. (2010). Design, simulation, and performance of a draft tube spout fluid bed coating system for aerogel particles. *Powder Technology*, *199*(2), 131–138.

Radl, S., Gonzales, B. C., Goniva, C., & Pirker, S. (2014). State of the art in mapping schemes for dilute and dense Euler–Lagrange simulations. *10th international conference on CFD in oil & gas, metallurgical and process industries*, 1–9.

Radl, S., & Sundaresan, S. (2014). A drag model for filtered Euler–Lagrange simulations of clustered gas–particle suspensions. *Chemical Engineering Science*, *117*, 416–425.

Salikov, V., Antonyuk, S., Heinrich, S., Sutkar, V. S., Deen, N. G., & Kuipers, J. A. M. (2015). Characterization and CFD-DEM modelling of a prismatic spouted bed. *Powder Technology*, *270*, 622–636.

Schneiderbauer, S., & Pirker, S. (2014). A coarse-grained two-fluid model for gas-solid fluidized beds. *The Journal of Computational Multiphase Flows*, *6*(1), 29–47.

Tsuji, Y., Tanaka, T., & Ishida, T. (1992). Lagrangian numerical simulation of plug flow of cohesionless particles in a horizontal pipe. *Powder Technology*, *71*(3), 239–250.

Macpherson, G. B., Nordin, N., & Weller, H. (2010). Particle tracking in unstructured, arbitrary polyhedral meshes for use in CFD and molecular dynamics. *Communications in Numerical Methods in Engineering*, *25*, 263–273.

Wang, C., Zhong, Z., & Jiaqiang, E. (2012). Flow regime recognition in spouted bed based on recurrence plot method. *Powder Technology*, *219*, 20–28.

Weller, H. G., Tabor, G., Jasak, H., & Fureby, C. (1998). A tensorial approach to computational continuum mechanics using object-oriented techniques. *Computers in Physics*, *12*(6), 620–631.

Wolff, M. F. H., Salikov, V., Antonyuk, S., Heinrich, S., & Schneider, G. A. (2014). Novel, highly-filled ceramic–polymer composites synthesized by a spouted bed spray granulation process. *Composites Science and Technology*, *90*, 154–159.

Zhou, Z. Y., Kuang, S. B., Chu, K. W., & Yu, A. B. (2010). Discrete particle simulation of particle–fluid flow: Model formulations and their applicability. *Journal of Fluid Mechanics*, *661*, 482–510.

Zhu, H. P., Zhou, Z. Y., Yang, R. Y., & Yu, A. B. (2007). Discrete particle simulation of particulate systems: Theoretical developments. *Chemical Engineering Science*, *62*(13), 3378–3396.